TISSUE ENGINEERING: Part A
Volume 21, Numbers 1 and 2, 2015

DOI: 10.1089/ten.tea.2014.0018

In Vitro and *In Vivo* Characterization of Pentaerythritol Triacrylate-co-Trimethylolpropane Nanocomposite Scaffolds as Potential Bone Augments and Grafts

Cong Chen, MS,[1,*] Leah Garber,[2,*] Mollie Smoak,[1] Carmel Fargason,[3] Thomas Scherr, PhD,[4] Caleb Blackburn,[2] Sasha Bacchus,[2] Mandi J. Lopez, PhD,[3] John A. Pojman, PhD,[2] Fabio Del Piero, PhD,[5] and Daniel. J. Hayes, PhD[1]

A thiol-acrylate-based copolymer synthesized via an amine-catalyzed Michael addition was studied *in vitro* and *in vivo* to assess its potential as an *in situ* polymerizing graft or augment in bone defect repair. The blends of hydroxyapatite (HA) with pentaerythritol triacrylate-co-trimethylolpropane (PETA), cast as solids or gas foamed as porous scaffolds, were evaluated in an effort to create a biodegradable osteogenic material for use as a bone-void-filling augment. Osteogenesis experiments were conducted with human adipose-derived mesenchymal stromal cells (hASCs) to determine the ability of the material to serve as an osteoinductive substrate. Poly(ε-caprolactone) (PCL) composites PCL:HA (80:20) (wt/wt%) served as the control scaffold, while the experimental scaffolds included PETA:HA (100:0), (85:15), (80:20), and (75:25) composites (wt/wt%). The results indicate that PETA:HA (80:20) foam composites had higher mechanical strength than the corresponding porous PCL:HA (80:20) scaffolds made by thermo-precipitation method, and in the case of foamed composites, increasing HA content directly correlated with increased yield strength. For cytotoxicity and osteogenesis experiments, hASCs cultured for 21 days on PETA:HA scaffolds in stromal medium displayed the greatest number of live cells compared with PCL:HA composites. Moreover, hASCs cultured on foamed PETA:HA (80:20) scaffolds resulted in the greatest mineralization, increased alkaline phosphatase (*ALP*) expression, and the highest osteocalcin (*OCN*) expression after 21 days. Overall, the PETA:HA (80:20) and PETA:HA (85:15) scaffolds, with 66.38% and 72.02% porosity, respectively, had higher mechanical strength and cytocompatibility compared with the PCL:HA control. The results of the 6-week *in vivo* biocompatibility study using a posterior lumbar spinal fusion model demonstrate that PETA:HA can be foamed *in vivo* without serious adverse effects at the surgical site. Additionally, it was demonstrated that cells migrate into the interconnected pore volume and are found within centers of ossification.

Introduction

For the past several decades, the standard treatment to augment or accelerate bone regeneration has been the implantation of bone grafts.[1] Allogeneic bone grafts are costly, require time-consuming bone banking procedures, and have the potential for disease transmission. Autogenous bone grafts have long been used as bone replacements but require additional surgeries, which increase the risk of donor site morbidity and the burden on health care providers.[2] Moreover, these techniques do not address the need for a clinically convenient and biodegradable method for conformally filling a critical-sized bone defect while providing mechanical support and biological cues necessary to promote bone regrowth. Artificial composite scaffolds, whether bioderived, synthetic, or hybrids, while studied extensively as alternatives for bone grafting and augmentation, have yet to see wide clinical adoption.[3] Composite structures with

[1]Department of Biological Engineering, Louisiana State University Agricultural Center, Louisiana State University, Baton Rouge, Louisiana.
[2]Department of Chemistry, Louisiana State University, Baton Rouge, Louisiana.
[3]Laboratory for Equine and Comparative Orthopedic Research, Department of Veterinary Clinical Sciences, School of Veterinary Medicine, Louisiana State University, Baton Rouge, Louisiana.
[4]Department of Chemical Engineering, Louisiana State University, Baton Rouge, Louisiana.
[5]Department of Pathobiological Sciences, School of Veterinary Medicine, Louisiana State University, Baton Rouge, Louisiana.
*These two authors contributed equally to this work.

calcium phosphates and magnesium silicates composing the bioactive ceramic portion have been studied thoroughly to improve both the mechanical and osteogenic properties of scaffolds but an *in situ* polymerizing, biodegradable bone augment or graft with biomimetic morphology and mechanical properties remains elusive.[3–5] An initial study conducted by our group demonstrated the formation of a porous interconnected scaffold derived from the product of an amine-catalyzed Michael addition polymerization reaction.[6] This thiol-acrylate reaction proceeds through a nonradical, step-growth process initiated by an amine/acrylate comonomer that is consumed in the reaction and incorporated into the growing polymer. Porous composite scaffolds made with this system were found to support human mesenchymal stromal/stem cell growth and to possess similar mechanical properties to cortical bone.[7]

The fabrication method of a scaffold can have a substantial impact on mechanical properties and biofunctionality by controlling porosity and interconnectivity. These factors influence cell attachment, proliferation, extracellular matrix production, and the transport of nutrients and wastes.[8–12] Solid freeform fabrication, thermal precipitation, gas foaming, and solvent casting followed by particulate leaching are the common approaches for making porous scaffolds for bone repair.[8,9] Except for gas foaming, these methods are not readily applicable to thermoset polymers due to their crosslinking densities and viscoelastic properties. Gas porogens and foaming apparatuses have the potential to be readily adapted to filling conformal defects in a clinical environment, similar to other surgical devices in use, such as fibrin sealant[13,14] and bone putty.[15]

Herein we report on the *in vitro* characterization of the mechanical and osteoinductive properties of a gas-foamed nanocomposite scaffold consisting of a thiol-acrylate copolymer with nanoscale hydroxyapatite (HA) inclusions. Scaffolds were prepared using a gas-phase propellant and foaming agent to investigate the relationship of scaffold composition to morphology, mechanical properties, cytocompatibility, and osteogenic properties. The impact of varying HA concentration in the pentaerythritol triacrylate-co-trimethylolpropane (PETA) polymer on morphology is illustrated using scanning electron microscopy (SEM) and micro-computed tomography (micro-CT) imaging. Mechanical testing was conducted to determine the compressive yield strength and modulus of the material. To evaluate cytocompatibility and osteogenic activity, human adipose-derived mesenchymal stromal cells (hASCs) were used as a model cell type. Metabolic activity, DNA content, calcium deposition, and the expression of the osteogenic markers alkaline phosphatase (*ALP*) and osteocalcin (*OCN*) were quantified with respect to scaffold composition. A 6-week *in vivo* study was also conducted to assess the basic biocompatibility of the foamed composite and the feasibility of *in situ* foaming for a boney fusion model.

Materials and Methods

Preparation of thiol-acrylate materials

All chemicals were used as received; trimethylolpropane tris(3-mercaptopropionate) (TMPTMP) was obtained from Sigma-Aldrich, diethylamine (DEA) (99% purity) from AGROS organics, and pentaerythritol triacrylate from Alfa Aesar.

Scaffolds were prepared by formulating PETA with 16.1% DEA and adding TMPTMP in a 1:1 molar functionality ratio, followed by mixing with a stir rod for 3 h as previously described.[6] Several concentrations of copolymer PETA with HA were studied; the first number in the abbreviation connotes the polymer content while the second number provides the amount of HA found in the composite as a wt/wt percentage (100:0, 85:15, 80:20, and 75:25). The mixtures were cast into cylindrical molds ($5 \times 10\,mm^2$) to form a solid scaffold. The foamed composite copolymer was prepared by pouring the PETA and HA (150 g in total) into a 250-mL pressurized canister using 7-g-compressed nitrous oxide as a gas foaming agent. The foamed composite copolymer was expelled into the same cylindrical molds used for solid casting.

Mechanical testing

Solid and foamed scaffolds, molded to 6 mm (diameter) × 12 mm (height) cylinder shape, were tested to determine maximal compressive strength and modulus. All scaffolds—solid, gas foamed, or thermally precipitated—were subjected to compression, and the ultimate compressive strength was reported at 30% strain. A universal testing machine (Instron Model 5696) was used at an extension rate of 0.5 mm/min.[6]

Morphological analysis

All of the scaffolds were placed on the EMS550X sputter coater, which applied a conductive platinum coating for 4 min followed by standard SEM analysis. Human cadaver bone from knee area was obtained under LSU exempted IRB protocol HE 13-10 from the Louisiana State University (LSU) Health Science Center.

Micro-CT analysis

Four PETA:HA (100:0), (85:15), (80:20), and (75:25) foams were fabricated by pressurized extrusion foaming and prepared as previously described.[6] The imaging was conducted at the Center for Advanced Microstructures and Devices (Louisiana State University) using a tomography beamline with 13 keV monochromatic X-rays with a 2.5 μm/px resolution. Projection exposure time varied from 2 to 4 s with $\Delta\theta = 0.25$ corresponding to the number of image slices (520). Reconstruction data were 16-bit signed integer with mean air intensity scaled to zero.

Avizo 7.0.1 (Visualization Services Group) generated the volume renderings from the three-dimensional (3D) data of the four foamed samples with two overlapping subvolumes displayed simultaneously. The blue-green colormap represents the HA inclusions, and the red-orange colormap represents the copolymer foam. Image J generated two-dimensional (2D) orthogonal slices possessing gray colormap settings using the same data with a scale equivalent to the 3D rendering. An approximate pore size was also measured using Image J. The orthogonal and micro-CT datasets were directly comparable, both as an aggregate dataset and as slices.

HA distribution and porosity calculation based on micro-CT

HA distribution analysis method is described in detail in Supplementary Data 1 section (Supplementary Data are available online at www.liebertpub.com/tea). To analyze the

porosity of the 3D data, 2D slices were read into a custom MATLAB code. For each slice the grayscale image was thresholded using Otsu's method[16] and then converted into a binary image. Morphological operations were performed to remove small imaging artifacts, and isolate interior and exterior pores. After quantifying solid and void pixels, porosity was calculated as follows: $\phi = \frac{V_{pores}}{V_{pores} + V_{solid}} \times 100\%$

Adult stem cell isolation and culture

Liposuction aspirates from subcutaneous adipose tissue were obtained from three healthy adult subjects (man = 1 and women = 2) undergoing elective procedures. All tissues were obtained with informed consent under a clinical protocol reviewed and approved by the institutional review board at the LSU Pennington Biomedical Research Center and used under an exempted protocol at LSU A&M College. Isolation of hASCs was performed as published previously.[12] Passage 2 of each individual was used for *in vitro* hASC osteogenesis evaluation on tissue-culture-treated plastic or on scaffolds of different compositions. In both cases, hASCs were cultured in either stromal (control—Dulbecco's modified Eagle's medium [DMEM], 10% fetal bovine serum [FBS], and 1% triple antibiotic solution) or osteogenic (DMEM, 10% FBS, 0.1 μM dexamethasone, 50 μM ascorbate-2-phosphate, 10 mM β-glycerophosphate, and 1% triple antibiotic solution) media for up to 21 days with media maintenance performed three times a week.

hASCs loading on scaffolds and culture

All types of scaffolds were either molded or sculpted into 5 mm (diameter) × 10 mm (height) cylinder shape and gas sterilized afterward. All the scaffolds were then submerged in stromal medium for 1 h before loading the hASCs. The same amount of second cell passages from all donors ($n = 3$) were pooled and directly loaded on a single face of each scaffold type at a concentration of 1.0×10^4 cells/μL for total volume of 5 μL. After 30 min of incubation in a saturated humidity atmosphere incubator at 37°C and 5% CO_2, the same volume of hASCs containing solution were directly applied on the opposite side of each scaffold as previously described.[12] Control groups included poly(ε-caprolactone) (PCL):HA (100:0 and 80:20) scaffolds. Experimental groups included PETA:HA (100:0, 85:15, 80:20, and 75:25) scaffolds. Scaffolds loaded with hASCs were immediately transferred to 48-well plates and cultured in stromal or osteogenic media for 21 days. Cell medium was changed every 2–3 days. Triplicates were performed for each assay.

In vitro *hASCs metabolic activity on scaffolds*

AlamarBlue™ (Life Technologies) is a useful measure of metabolic activity and is frequently used as an analog of cell viability and proliferation. All scaffold samples were seeded with hASCs and cultured in stromal or osteogenic media for 21 days. The AlamarBlue™ conversion was measured at 7, 14, and 21 days. The scaffolds were removed from culture, washed three times in phosphate-buffered saline, and incubated with 10% AlamarBlue in Hank's balanced salt solution without phenol red (pH 7) for 90 min. The fluorescence of three aliquots (100 μL) from each scaffold was measured at an excitation wavelength of 530 nm and an emission wavelength of 595 nm using a fluorescence plate reader (Wallac 1420 multilabel HTS counter).

Alizarin red staining

hASCs calcium deposition (triplicates of scaffolds alone and cell-scaffolds) was assessed after 7, 14, and 21 days of culture in control or osteogenic medium based on alizarin red staining. Wells were washed with 0.9% NaCl and fixed with 70% ethanol. Wells were stained with 2% alizarin red for 10 min and washed with deionized water. Wells were destained with 10% cetylpyridinium chloride monohydrate for 4 h at room temperature with constant agitation. Results were normalized to values from scaffolds cultured without cells for the same time periods.

In vitro *quantification of DNA on scaffolds*

Total DNA content was used to determine the number of cells on each scaffold as previously described.[17] After triplicates of each scaffold were minced by a scalpel and the DNA was digested with 0.5 mL of 0.5 mg/mL proteinase K (Sigma-Aldrich) at 56°C overnight, aliquots (50 μL) were mixed with equal volumes of 0.1 g/mL Picogreen dye solution (Invitrogen) in 96-well plates. Samples were then excited at 480 nm with a plate reader (Wallac 1420 multilabel HTS counter). Scaffolds without cells were used as negative controls.

Quantitative real-time polymerase chain reaction

Total RNA was extracted from triplicates of cell-scaffold constructs as previously described.[12] cDNA was synthesized from total RNA using EcoDry Premix (ClonTech). Real-time quantitative reverse transcription polymerase chain reaction was performed using 2 × iTaq™ SYBR® green supermix with ROX (Bio-Rad) and primers for *ALP* and *OCN*[12] to quantify osteogenic target gene expression of hASCs loaded to scaffolds and cultured in either stromal or osteogenic media for 7, 14, and 21 days. Reactions were performed with an MJ Mini™ Thermal Cycler (Bio-Rad). The sequences of PCR primers (forward and backward, 50–30) were as follows: ALP, 5′-AATATGCCCTGGAGCT TCAGAA-3′ and 5′-CCATCCCATCTCCCAGGAA-3′; OCN, 5′-GCCCAGCGGTGCAGAGT-3′ and 5′-TAGCGCCTGGGT CTCTTCAC-3′. Samples were normalized (ΔCt) against the house keeping gene 18S rRNA and the $-\Delta\Delta$Ct value of *ALP* and *OCN* in scaffolds cultured in osteogenic and control media was calculated using the ΔΔCt method.[18]

Statistical analysis

All results were expressed as mean ± standard error of mean. Data were analyzed with one-way analysis of variance, followed by Tukey's minimum significant difference *post hoc* test for pairwise comparisons of main effects. For all comparisons, a p-value < 0.05 was considered significant.

In vivo *study*

Scaffold preparation and surgical implantation. Five male Fischer rats (Harlan Sprague-Dawley) were randomly assigned to three different treatments: (i) one rat was implanted with presculpted PETA + 20% HA, (ii) three rats were implanted with PETA + 20% foamed *in situ*, or (iii) one rat was

implanted with PETA + 0% HA foamed *in situ*. Stock/HA and TMPTMP/HA prepolymer mixture was placed into a 250-mL pressurized spray canister with 7-g-compressed nitrous oxide as a gas foaming agent. The foamed composite copolymer was expelled from the canister onto a sterile surface. The solid composite was cut into a rectangle with dimensions ($15 \times 10 \times 1\,mm^3$) for rat number 1. For rats 2, 3, and 4, the prepolymer mixture was prepared as described previously and foamed into a 5-mL syringe for surgical application. The process was the same for rat 5, but the formulation did not contain HA.

The rat posterolateral lumbar spinal fusion surgery was performed as previously described.[19] Prior to general anesthesia, rats received a subcutaneous injection of 0.5 mg/kg butorphanol (Torbugesic; Fort Dodge Animal Health) and 0.02 mg/kg glycopyrrolate (Robinul-V; Fort Dodge Animal Health). Isoflurane was administered 20 min later in an induction chamber to induce anesthesia. The isoflurane was maintained at 1.5% via nose cone on a Bain circuit for the remainder of the procedure. The lumbar region was clipped and aseptically prepared with 70% isopropanol and betadine. A posterior midline skin incision was made over the lumbar spine. Two fascial incisions were made 3-mm lateral and parallel to the dorsal spinus processes. The L4 and L5 transverse processes were exposed with sharp and blunt dissection. A scalpel was used to decorticate each transverse process. Surgical sites were thoroughly lavaged with physiologic saline. In rat 1, solid scaffolds were placed adjacent to both sides of the spine such that they spanned between the midpoint of each transverse process. For the remaining rats, 3 mL of each foamed scaffold was applied so that scaffold spanned between the center of each transverse process next to the spine. Fascial and subcutaneous incisions were closed separately with 3-0 polyglactin 910 (Vicryl; Ethicon) in a simple continuous pattern. Closure of the fascia around the implants effectively filled any potential space. A subcutaneous/subcuticular suture pattern was used to approximate skin edges, and tissue adhesive was used for skin closure (Vetbond; 3M). Scaffolds were harvested 3 weeks (rat 3) or 6 weeks (rats 1, 2, 4, and 5) after implantation following euthanasia by CO_2 asphyxiation.[20] At 3 weeks, no significant results were shown in radiographs, micro-CT, or histology analysis. Therefore, no results from rat 3 were reported in the ''Results'' and ''Discussion'' sections.

Micro-CT analysis. Immediately postmortem, 2D micro-CT imaging was performed (40 kV and 540 ms) to obtain 0.04-mm slices every 0.9° throughout a 360° rotation (SkyScan 1074; Skyscan n.v.). Three-dimensional files were reconstructed from 2D images. Measurements of 2D and 3D images were performed with Avizo® Standard packages (FEI™ Visualization Sciences Group).

A density line was first drawn in void space with no tissue to measure the optical density (OD) of the image background. The line was then moved to L3 of the specimen's vertebral column to determine the OD of the tissue unaffected by the surgery. Lastly, the density line was moved between L4 and L5 of the specimen's vertebral column to calculate the OD of the area treated by the scaffolds. The density of the area treated by the implant was normalized by the densities of the void space and the unaffected bone region in order to calculate the percentage of bone growth present in each specimen.[20]

$$OD = \log \frac{255}{Pixel\ value} \qquad \frac{OD_{Treated}}{OD_{Untreated}} \times 100 = \%\ new\ growth$$

Histology. Following imaging, spines were cut into half and fixed in neutral buffered formalin. One half of each spine was decalcified and paraffin embedded and longitudinal sections (5 μm) were stained with hematoxylin and eosin. Microarchitecture was evaluated using Olympus BX46 microscope.

Results

SEM analysis

The foamed scaffold samples were analyzed using SEM to examine the trends in morphology. The morphology of the foam containing 0–20% HA was similar to cancellous human cadaver bone (Fig. 1). The average pore diameters of PETA:HA 100:0 and 85:15 scaffolds were 250–300 μm, with no significant difference between the two. PETA:HA 80:20 had a slightly smaller pore diameter of 150–200 μm. The pore diameter of PETA:HA 75:25 was only 70–100 μm. PETA:HA 70:30 had a pore diameter of < 50 μm. It is apparent from Figure 1 that HA does not affect pore size significantly until the HA content reaches 25% or greater. The viscosity of the polymer mixture during the fabrication

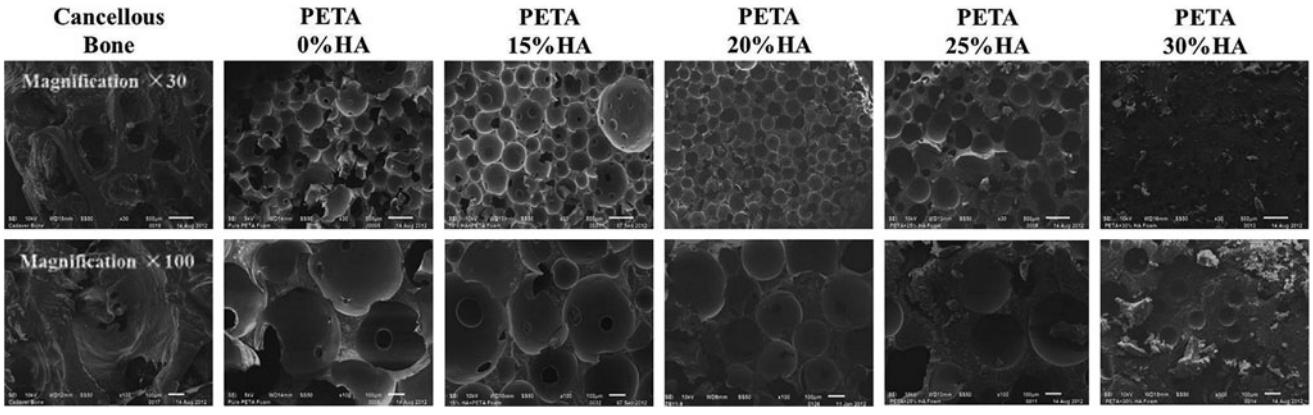

FIG. 1. Scanning electron microscopy analysis of pentaerythritol triacrylate-co-trimethylolpropane (PETA):hydroxyapatite (HA) (100:0), (85:15), (80:20), and (75:25) scaffolds.

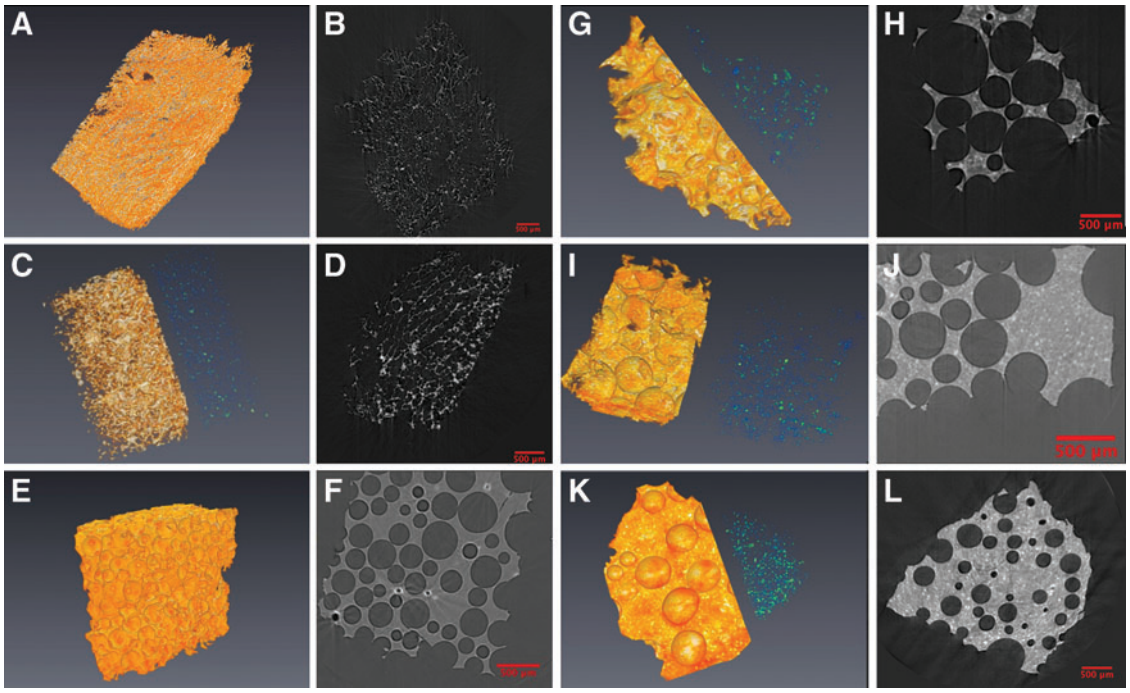

FIG. 2. Avizo rendering pictures (three-dimensional and two-dimensional [2D]) of micro-computed tomography (micro-CT) data of scaffolds. The blue-green colormap represents the HA inclusions, and the red-orange colormap represents the copolymer foam. **(A, B)** Poly(ε-caprolactone) (PCL):HA (100:0), **(C, D)** PCL:HA (80:20), **(E, F)** PETA:HA (100:0), **(G, H)** PETA:HA (85:15), **(I, J)** PETA:HA (80:20), **(K, L)** and PETA:HA (75:25) scaffolds. Each scale bar in the 2D pictures indicates 500 μm. Color images available online at www.liebertpub.com/tea

process increased, reducing N_2O expansion in the polymer mixture. Additionally, HA content above 25% causes increased pore wall thickness and an apparent reduction in scaffold interconnectivity.

Micro-CT analysis, HA distribution, and porosity calculation

There is a limitation associated with the amount of material that SEM can qualitatively analyze, reducing the generalizability of the data. To address this limitation, the interconnectivity, pore volume, and ceramic phase distribution of HA-PETA copolymer composites and PCL (control) were further analyzed by micro-CT. Micro-CT image analysis is a more sensitive method for estimating porosity of materials when compared to SEM, flow porosimetry, and gas adsorption.[21] Volume renderings (Fig. 2) were generated from PETA and PCL composite foam 3D data using Avizo 7.0.1 (Visualization Services Group). Two overlapping subvolumes were rendered simultaneously, one with a red-orange-white colormap corresponding to thiol-acrylate foam, and another with a blue-green colormap corresponding to ceramic HA additives. For PETA:HA (85:15, 80:20, and 75:25), ceramics on average are 183.4 ± 93.9, 221.3 ± 102.3, and 206.8 ± 114.7 voxels away from an edge of the scaffold while they are 282.7 ± 91.6, 355.9 ± 114.7, and 336.8 ± 101.8 voxels away from the center of the scaffold, respectively. For all types of PETA:HA scaffolds, the HA ceramics were on average closer to the edge of the scaffold than to the center of it, indicating that ceramic particles were evenly distributed rather than clustered around the center of the scaffolds. Figure 3 shows HA histograms of the distance from each ceramic to the center

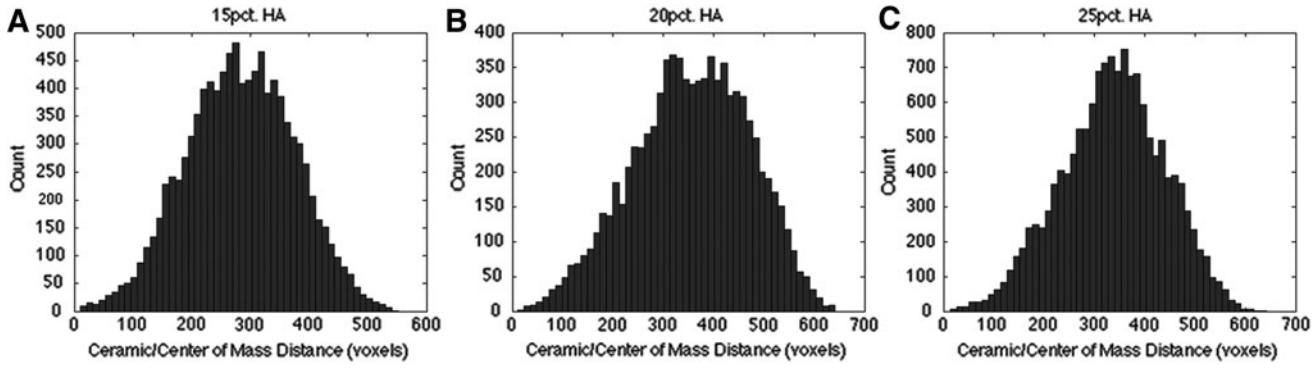

FIG. 3. HA histograms of distance from each ceramic to the center of mass of the scaffold. **(A)** PETA:HA (85:15), **(B)** PETA:HA (80:20), and **(C)** PETA:HA (75:25).

of mass of the scaffold; they display a very Gaussian-looking distribution around the mean. This indicates that there are nearly equal amounts of ceramics distributed spatially around this mean distance.

The porosity of PETA:HA (100:0, 85:15, and 80:20) is 66.9%, 72.0%, and 66.4%, respectively (Fig. 4A). It should be noted that an apparent transition in morphology occurred between 20% and 25% HA inclusions. As HA concentration increased from 20% to 25%, the porosity decreased significantly from 66.4% to 44.7%. When HA concentration reaches 25%, the pore size is substantially reduced and the interconnected void volume appeared to decrease, resulting in a structure similar to a closed-cell foam (Fig. 2K, L). This is attributed to increased polymer solution viscosity correlated with reduced N_2O expansion and mobility. In addition, the inclusion of 20% HA to PCL scaffolds increased the porosity from 78.0% (PCL:HA 100:0) to 87.6% (PCL:HA 80:20) (Fig. 2A, C).

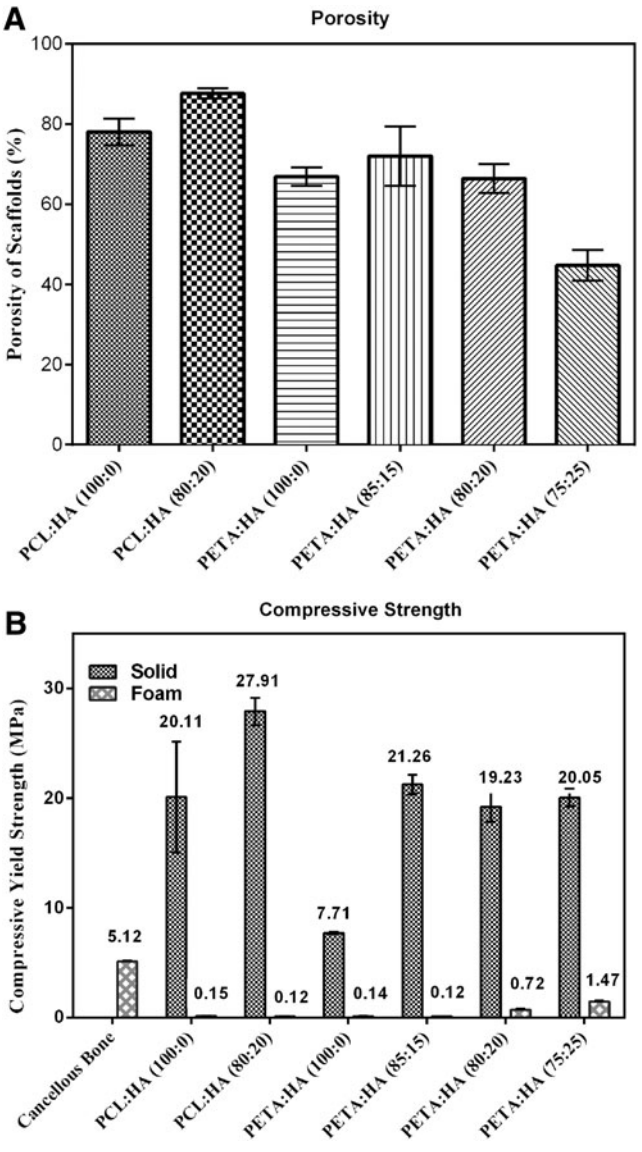

FIG. 4. **(A)** Porosity of PETA:HA (100:0), (85:15), (80:20), and (75:25) scaffolds; **(B)** maximum compressive strength of PETA:HA (100:0), (85:15), (80:20), and (75:25) composites (*solid* and *foam*).

Mechanical testing

Figure 4B shows the compressive yield strength of the foamed and solid PCL:HA (100:0 and 80:20) and PETA:HA (100:0, 85:15, 80:20, and 75:25) samples. Compressive strength of solid PCL:HA (100:0 and 80:20) samples is significantly higher than corresponding PETA:HA (100:0 and 80:20) samples. When comparing among porous scaffolds, PETA:HA (100:0 and 80:20) scaffolds are either the same as or stronger than PCL:HA (100:0 and 80:20). The compressive strength of the foamed PETA:HA steadily increased with increasing HA content; however, the solid samples did not follow a similar trend. The addition of 15% HA in the foam resulted in a significant increase in compressive strength compared with the control samples and increasing the HA content beyond 15% correlated with increased compressive strength. Conversely, solid PETA:HA (85:15, 80:20, and 75:25) composite scaffolds exhibited approximately the same compressive strength for all HA-containing samples. It is believed that the porosity (Fig. 4A) is responsible for the different trends between solid and foamed scaffolds.

hASCs metabolic activity and proliferation on scaffolds cultured in control and osteogenic media

For cell-scaffold constructs cultured in stromal media, PETA:HA (100:0) had the highest metabolic activity after 14 days of culture. PCL:HA (100:0) had the highest levels of metabolic activity after 21 days of culture in stromal medium and no significant differences were observed from this scaffold between any time point. In osteogenic media, PETA:HA (100:0) scaffolds again exhibited the highest metabolic activity after 7, 14, and 21 days of culture. PETA:HA (85:15 and 80:20) scaffolds had the next highest metabolic activity at all time points. PCL scaffolds showed the lowest levels of metabolic activity after 7, 14, and 21 days of culture (Fig. 5A). The addition of HA to PETA and PCL scaffolds decreased metabolic activity on constructs cultured in stromal and osteogenic media. Significantly higher metabolic activity was observed at all time points for PCL:HA (100:0) and PCL:HA (80:20) scaffolds cultured in stromal media compared with osteogenic media. This data is in agreement with previous studies that indicate that the metabolic activity of hASCs is expected to decrease as cells commit to an osteogenic lineage.[12,22] No differences in metabolic activity were seen in PETA:HA composite samples between stromal and osteogenic conditions. hASCs cultured on HA-containing scaffolds were expected to begin differentiation into an osteogenic linage regardless of the media condition, potentially accounting for the differences in metabolic activity between HA-containing and control samples with respect to media condition. Almost no metabolic activity was measured in PETA:HA (75:25) scaffolds, likely as a result of the reduced pore size and interconnectivity.

Total DNA content was quantified using Quant-iT™ PicoGreen®, to analyze the hASC proliferation in scaffolds. Differences in DNA content, between stromal and osteogenic media conditions, were observed at the 7-day culture time point for PCL:HA (80:20), PETA:HA (85:15), and PETA:HA (80:20) composite scaffolds. When comparing

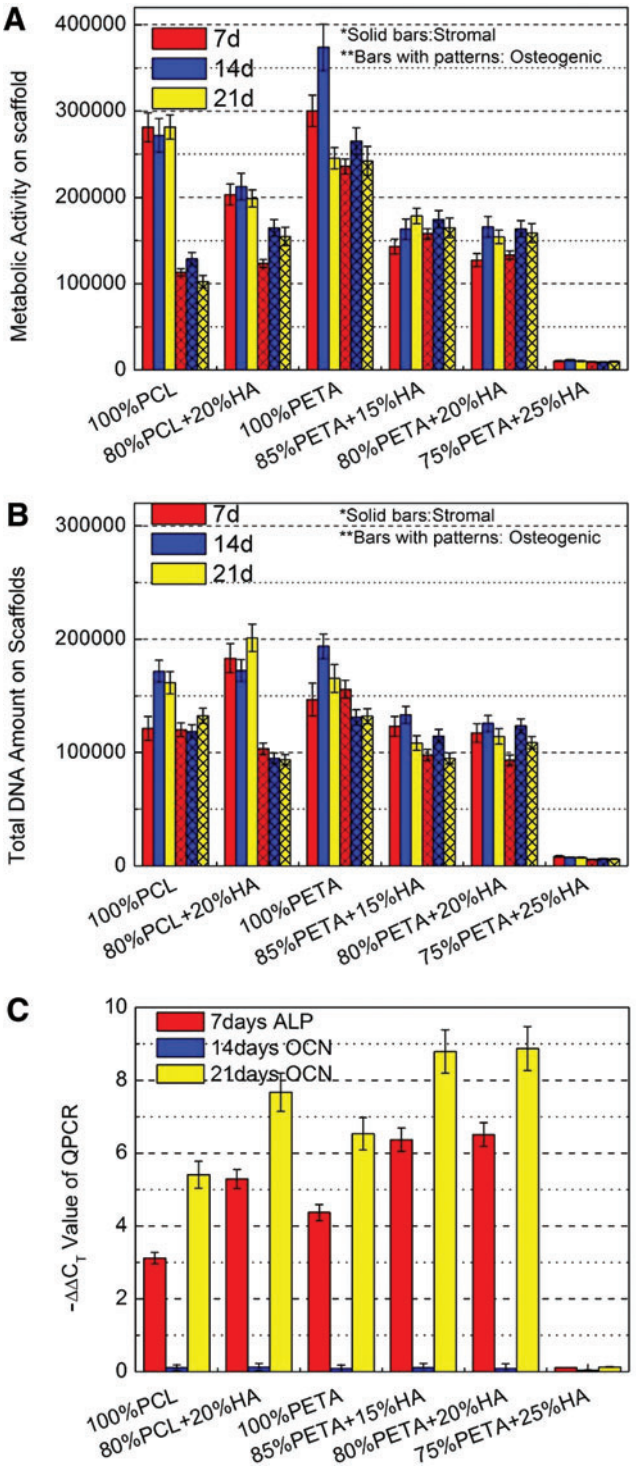

FIG. 5. **(A)** Relative metabolic activity of human adipose-derived mesenchymal stromal cells (hASCs) on PETA:HA (100:0), (85:15), (80:20), and (75:25) scaffolds; **(B)** relative DNA content of hASCs on PETA:HA (100:0), (85:15), (80:20), and (75:25) scaffolds; **(C)** real-time quantitative reverse transcription polymerase chain reaction analysis of alkaline phosphatase (ALP) (7 days) and osteocalcin (OCN) (14 and 21 days) expression from hASCs on PETA:HA (100:0), (85:15), (80:20), and (75:25) scaffolds. Color images available online at www.liebertpub.com/tea

samples within the stromal media treatment condition, it can be observed that the PETA:HA samples had significantly fewer cells than the PCL or PETA control. The most pronounced difference in DNA content was between PCL:HA (80:20) composites and PETA:HA scaffolds in stromal media conditions (Fig. 5B), where the DNA content in PCL (80:20) scaffolds was significantly higher than PETA:HA composites. At 14 and 21 days, levels of DNA content observed in both PCL scaffolds and the pure PETA scaffolds were significantly higher than the PETA:HA composites, in stromal media conditions. Within the osteogenic media treatment groups, the PETA:HA scaffolds showed slightly increased DNA content compared with the PCL:HA scaffolds, but all scaffolds contained a similar number of cells.

Quantitative real-time polymerase chain reaction

Bone morphogenic proteins, known to regulate osteogenesis, act on the transcription factor core binding factor alpha 1 (Cbfa1) and result in the activation of osteoblast-related genes, such as *ALP* and *OCN*.[17,23] The expression of these genes is commonly used as early and middle stage markers of osteogenesis, respectively.[24] Quantitative real-time polymerase chain reaction was used to assess the expression of *ALP* at the 7-day time point and *OCN* at 14- and 21-day time points (Fig. 5C). Based on previous studies, *ALP* expression in hASCs decreased dramatically after 7 days in culture and was therefore not measured at the 14- and 21-day time points in this study.[12,24] The differences in the expression of *ALP* and *OCN* in hASCs cultured on scaffolds in stromal and osteogenic media are represented in Figure 5C. The cells on PETA:HA (85:15) and PETA:HA (80:20) scaffolds showed similar expression of *ALP* at 7 days and were significantly higher than all other PETA and PCL scaffolds. Additionally, hASCs on pure PETA scaffolds had higher *ALP* expression than pure PCL control scaffolds. While hASCs cultured on PCL:HA (80:20) scaffolds had higher *ALP* expression than pure PETA or PCL, the expression was still lower than PETA:HA (85:15) and PETA:HA (80:20) scaffolds. Moreover, the expression of the *OCN* marker could only be observed at 21 days of culture, with little expression at 14 days regardless of treatment. The *OCN* expression level demonstrated in hASCs as a function of scaffold type was similar to that of *ALP* expression with maximal *OCN* expression observed in PETA:HA (85:15) and PETA:HA (80:20) followed closely by *OCN* levels in PCL:HA composites. Consistent with the previously described results, cells cultured on the PETA:HA (75:25) sample did not demonstrate substantial expression of either marker, likely the result of poor cell proliferation/survival associated with the lack of a porous and interconnected structure.

Calcium deposition in hASCs cultured in control and osteogenic media

The mineralization of different scaffold types was assessed using alizarin red staining, which stains calcium-rich deposits. hASCs cultured on the PETA composites in stromal and osteogenic media were tested against PCL and PCL:HA scaffolds (Fig. 6A). As expected, alizarin red staining was significantly higher in hASCs cultured in osteogenic media compared with samples cultured in stromal media.[12] Also, hASCs cultured in osteogenic media showed

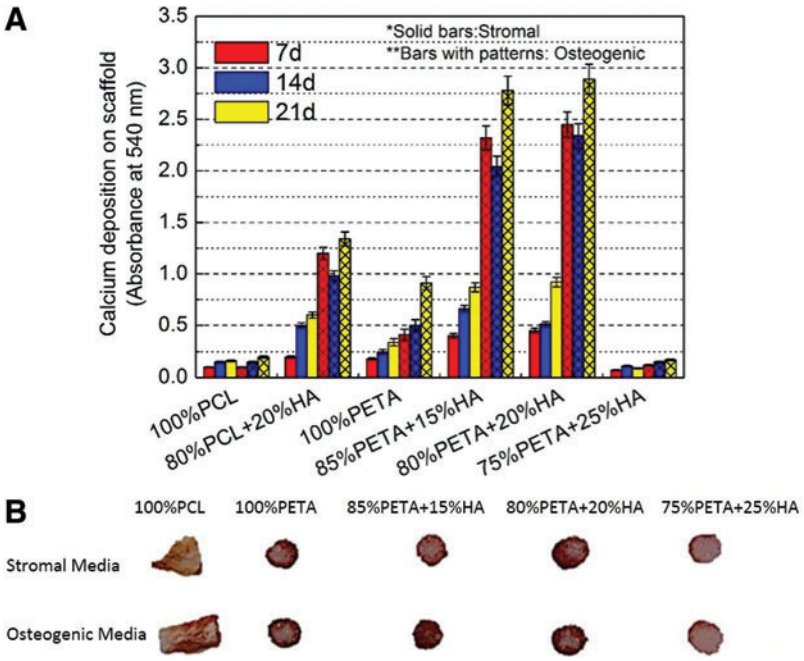

FIG. 6. Alizarin red stain of PETA:HA as a function of scaffold composition, media treatment, and time. **(A)** Quantitative analysis of staining on scaffolds loaded with hASCs and cultured in stromal and osteogenic media for 7, 14, and 21 days. **(B)** Cross-section of each type of scaffold stained with alizarin red on 21 days. Color images available online at www.liebertpub.com/tea

a significant increase in staining with respect to increased time in culture. Except for PETA:HA (75:25), all scaffolds showed significant differences in the calcium deposition at 14 days between stromal and osteogenic media. Both PETA:HA (80:20) and PETA:HA (85:15) cultured in osteogenic media demonstrated significantly increased staining compared with all other experimental samples and controls. Almost no calcium deposition, however, was observed at 14- and 21-day culture time points in PETA:HA (75:25) (Supplementary Fig. S13).

In vivo *study*

Radiography. Observed behavior and weight gain were normal (90.7 ± 5.9 g) for all rats after surgery. Foamed thiol-acrylate nanocomposite implants showed some increase in radiographically detectable opacity 3 weeks after implantation compared with immediately after surgery, and the opacity increased further by 6 weeks after implantation. The increasing intensity of bone scaffolds is consistent with scaffold calcification (Fig. 7). Rats implanted with

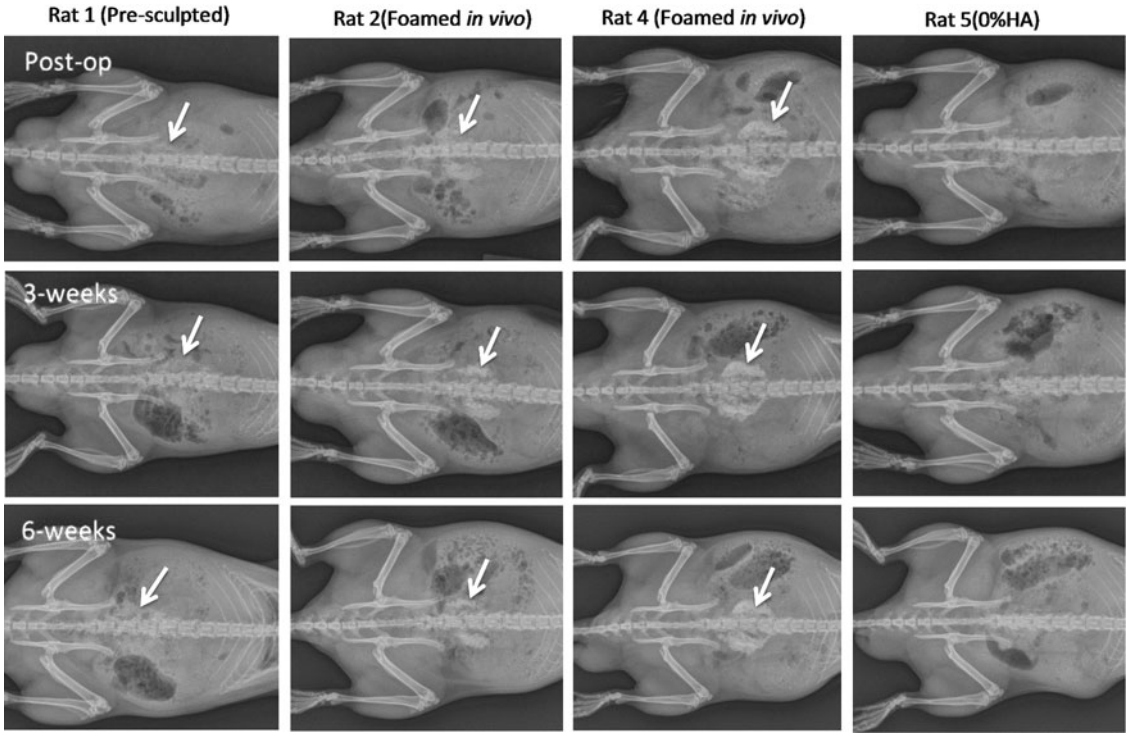

FIG. 7. Radiographs of *in vivo* study. Arrows denote location of PETA:HA implants.

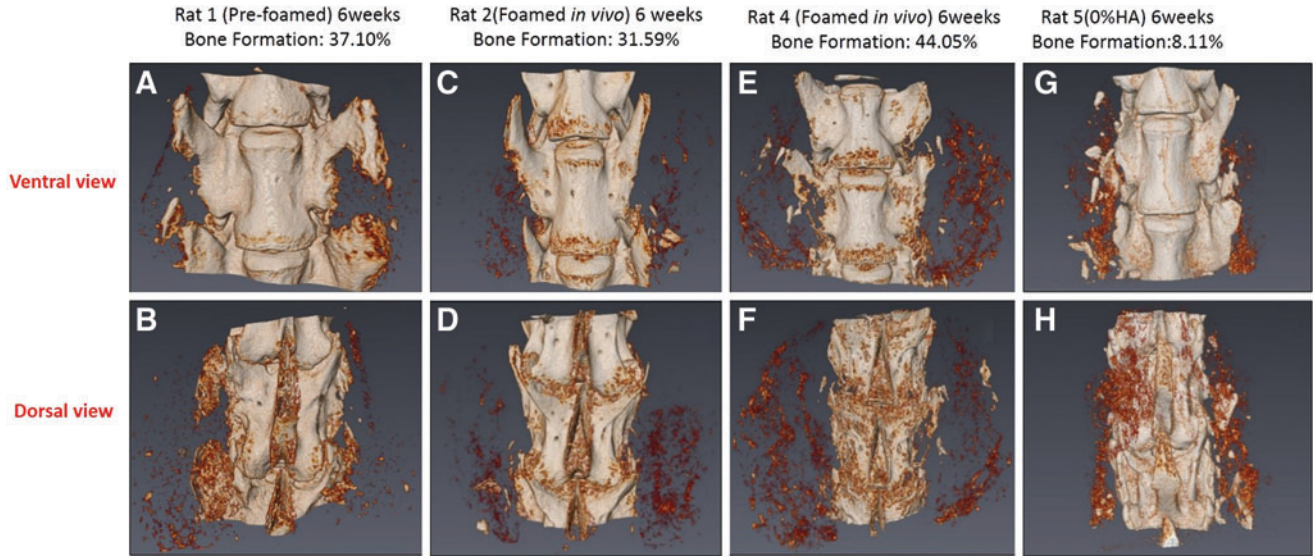

FIG. 8. Micro-CT data of the L4 (top) and L5 (bottom) vertebral bodies from the *in vivo* study. The light-colored regions indicate densification in scaffolds. Color images available online at www.liebertpub.com/tea

premolded samples had a lower increase in radioopacity by 6 weeks after implantation compared with rats implanted with PETA + HA foamed *in situ*. No evidence of calcification was observed in implants of 0% HA presculpted PETA. This is consistent with the *in vitro* osteogenesis target gene expression results.

Micro-computed tomography. The micro-CT results support the radiographic findings. The light-colored regions indicate densification in the scaffolds in Figure 8. *In-vivo* and *in-situ*-polymerized scaffolds had the greatest amount of densification 6 weeks after surgery.

Analysis of bone formation using histology. Histological examination was performed on presculpted PETA:HA (80:20) and PETA:HA (80:20) foamed *in situ*, and PETA:HA (100:0) foamed *in situ*. The essential step of decalcifying and staining the spinal column poses a problem in analyzing tissues for bone formation evaluating the calcified areas. For this reason, tissue morphology is considered a reliable parameter to measure bone formation.[25] Each cohort was examined 6 weeks postoperative.

Treatment cohort 1 [presculpted PETA:HA (80:20)] proved to be biocompatible, support cell growth, and induce osteogenesis in tissue growing into the foam structure.

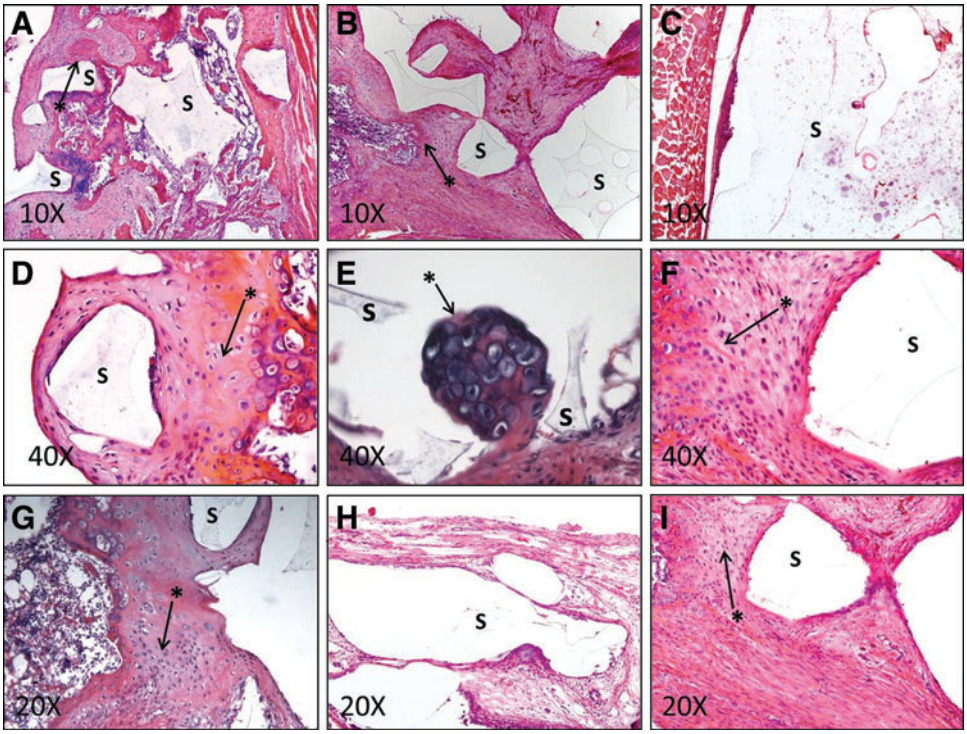

FIG. 9. Histology analysis using hematoxylin and eosin staining. A medial cut was made on the spinal column of each rat. The progress of this specimen guides the analysis of the other specimens. Arrows denote areas of endochondral ossification. **(A, B, D, F,** and **I)** Rat was treated with the presculpted PETA:HA (80:20) scaffold. **(C, E,** and **G)** Rats were treated with PETA:HA (80:20) scaffold foamed *in situ*. **(H)** Rat was treated with PETA:HA (100:0) foamed *in situ*. S, scaffold implants; *, site endochondral ossification. Color images available online at www.liebertpub.com/tea

Figure 9A shows that the PETA:HA (80:20) implant is partially demarcated by fibrosis and multifocal fibrocartilage formation, which incorporates multifocal, small areas of endochondral ossification. Figure 9D contains the implant surrounded by fibrous tissue, fibrocartilage, and peripheral endochondral ossification. The appearance of cells chondrocytic in appearance, a tide mark, and an ossified site present around the implant site indicate that the PETA:HA (80:20) scaffold has the potential to induce endochondral ossification. Figure 9B shows that the polymer implant is segmentally demarcated by fibrous and fibrocartilagenous tissues with an ossified rim blending into pre-existing trabecular bone. The findings in Figure 9B are further supported by Figure 9I and F.

Treatment 2 (PETA:HA 80:20 *in situ*) was also shown to be biocompatible, support bone growth, and induce osteogenic differentiation. In cohort 2, histological changes are characterized by osteogenic activity around the implant site. Figure 9C shows a large accumulation of polymer implant near the skeletal muscle of the rat, surrounded by a thin layer of fibrous tissue with a focal area also containing macrophages. Figure 9E shows the presence of a cavitation lined by one to three layers of spindled cells (fibroblasts) containing the scaffold and a sprouting nidus of endochondral ossification. Figure 9G shows that in the area adjacent to the polymer-occupied cavitation, there are fibrous tissues and a region of endochondral ossification.

Histological analysis of cohort-3 PETA:HA (100:0) indicates that the lack of nanoscale HA reduces the osteogenic properties of the scaffolds. In Figure 9H, the scaffold is surrounded by a very thin layer of fibrous tissue, indicating a reduction in the formation of organized tissue in the implant region.

Discussion

Bone tissue engineering involving polymer/ceramic composites presents an attractive alternative approach to the repair and regeneration of damaged or traumatized bone tissue.[1,26] Several studies have previously explored the potential use of thiol-acrylate chemistry for biomedical devices, but radical-based photoinitiators are usually used to drive the polymerization process.[12,27,28] A nonradical-based polymerization method is potentially less cytotoxic and therefore more amenable to *in situ* polymerization. The amine-catalyzed Michael addition for thiol-acrylate polymerization described in this study has potential advantages compared to photoinitiated reactions because the chain propagation does not require a free radical initiator during the polymerization reaction. The mechanism of this amine-catalyzed reaction has been previously investigated.[6,29] The general reaction occurs via the formation of a catalyst/comonomer molecule by the Michael addition of a secondary amine across the alkene end group found in acrylate monomers. The *in situ* catalyst produced reacts with a trifunctional thiol and trifunctional acrylates forming a high-density crosslinked copolymer. The step growth nature and the incorporation of the tertiary amine catalyst reduce concerns about potential leaching of free radical initiators and unreacted monomer. This reaction, therefore, is potentially more attractive for *in situ* polymerization for bone formation than comparative free-radical-based methods.

The PCL-based scaffold was synthesized via a thermal precipitation method resulting in pore size, volume, and interconnectivity that are largely independent of solution viscosity.[30] Results showed that such characteristics were directly influenced by the viscosity of the stock solution in the polymerization of PETA composites.[31] It is well documented that an interconnected pore structure can help support cell migration, cell differentiation, nutrient transport,[32,33] and, in some cases, formation of blood vessels.[34–36] Because HA was found to decrease interconnectivity, it was expected that the highest HA concentration sample PETA:HA (75:25) would not provide a suitable environment for cell in-growth and nutrient/waste transport. Electron microscopy images and micro-CT analysis indicate that PETA:HA (75:25) scaffolds lack interconnectivity of the void volume providing for cell penetration and nutrient/waste transport required for cell growth and differentiation. The analysis of cell viability and expression of osteogenic markers further supported this hypothesis.

The decreased metabolic activity of PETA:HA composites compared with the PETA control is likely related to differences in cell function, not cell number, attributed to osteogenic differentiation of hASCs. The decreased cell proliferation and metabolic activity also had an inverse relationship with the increased calcium deposition and expression of osteogenic markers. This data further supports the hypothesis that HA induces osteogenesis, resulting in decreased metabolic activity and proliferation.[37,38]

Calcium deposition correlated with the expression of *ALP* and *OCN* in hASCs cultured on PETA:HA (85:15) and PETA:HA (80:20) scaffolds, which were significantly greater than PCL:HA (80:20), pure PCL, and PETA control scaffolds in both media conditions, providing a further indication that scaffolds composed of PETA may be an appropriate material for the repair of bone defects. Increased alizarin stain uptake in PETA:HA (80:20) and PETA:HA (85:15), compared with PCL:HA (80:20), does not correlate with increased cell density or metabolic activity but does correlates with increased *ALP* and *OCN* expression. PETA is better able to induce the expression of osteogenic markers than PCL, but further comparisons at differing concentrations and with other degradable resins are required to test this hypothesis. Cross-sectional images of PETA:HA (75:25) scaffolds demonstrate poor alizarin red penetration, providing further support that the void volume is not substantially interconnected.

Although increasing HA content resulted in reduced pore size and interconnectivity, it provided a more solid and stronger structure for the scaffold. Other studies have shown a similar trend of decreasing porosity with increasing HA content.[39] The increase in compressive strength seen in solid samples is predictable and similar to that seen with other nanoscale polymer fillers.[40,41] As porosity played no role in the solid samples, the increase in viscosity with increasing HA content beyond 15% did not significantly affect the mechanical strength.

Histological results demonstrated that both the presculpted and foamed *in situ* PETA:HA (80:20) scaffolds induced endochondral ossification. Radiography results indicating increased densification further supported these findings. During the *in vivo* study, the structure of the *in-situ*-polymerized foam sample may have been disrupted when the surgical site was closed during the surgery. Poor

porosity and interconnectivity could be the reason why the densified regions of the radiographs were noncontinuous. Overall results suggest that PETA:HA scaffolds could be a suitable substrate for bone regeneration.

Conclusions

By gas foaming thiol-acrylate-based copolymers that were synthesized via Michael addition with an *in situ* amine catalyst, a porous polymeric scaffold with bone-like morphology was developed as a potential graft or augment in critical-sized bone defect repair. Not only does PETA:HA composite has substantial porosity and interconnectivity, it also demonstrates adequate mechanical strength as compared to cortical bone. Compared with PCL:HA composites, both PETA:HA (85:15) and PETA:HA (80:20) scaffolds showed higher mineral deposition and *ALP* and *OCN* expression level. Overall, the PETA:HA had higher compressive strength and improved cytocompatibility compared with PCL controls. Mesenchymal cells cultured on PETA-based scaffolds had a greater expression of osteogenic markers and the scaffolds exhibited significantly greater mineralization than hASCs cultured on PCL controls. The *in vivo* study demonstrated that animals injected with PETA:HA composites showed no signs of surgical site or systemic toxicity and that PETA:HA composites induced osteogenesis *in vivo*. Additionally, the study serves as a proof-of-concept that gas foaming of thiol-acrylate polymers *in vivo* may be used to conformally fill irregular-sized defects.

Acknowledgments

The authors would like to thank Dr. Jeffery Gimble (Pennington Biomedical Research Center, Tulane University, and LaCell) for his continued support and for supplying our project with hASCs. We would also like to thank Nan Zhang and Hal Holloway for their assistance in the *in vivo* characterization. We would also like to give special thanks to Dr. Todd Monroe for the use of his laboratory and resources. The National Science Foundation grants (Proposal numbers CMMI-963482 and CBET-1254281) and from LSU AgCenter provided financial support for this research.

Disclosure Statement

No competing financial interests exist.

References

1. Pallua, N., and Suscheck, C.V. Tissue Engineering: From Lab to Clinic. Berlin: Springer Verlag, 2010.
2. Ahlmann, E., Patzakis, M., Roidis, N., Shepherd, L., and Holtom, P. Comparison of anterior and posterior iliac crest bone grafts in terms of harvest-site morbidity and functional outcomes. J Bone Joint Surg Am **84-A,** 716, 2002.
3. Zanetti, A.S., Sabliov, C., Gimble, J.M., and Hayes, D.J. Human adipose-derived stem cells and three-dimensional scaffold constructs: a review of the biomaterials and models currently used for bone regeneration. J Biomed Mater Res B Appl Biomater **101,** 187, 2013.
4. Hutmacher, D.W. Scaffolds in tissue engineering bone and cartilage. Biomaterials **21,** 2529, 2000.
5. Bohner, M. Resorbable biomaterials as bone graft substitutes. Mater Today **13,** 24, 2010.
6. Garber, L., Chen, C., Kilchrist, K.V., Bounds, C., Pojman, J.A., and Hayes, D. Thiol-acrylate nanocomposite foams for critical size bone defect repair: A novel biomaterial. J Biomed Mater Res A **10,** 3531, 2013.
7. Sundelacruz, S., and Kaplan, D.L. Stem cell- and scaffold-based tissue engineering approaches to osteochondral regenerative medicine. Semin Cell Dev Biol **20,** 646, 2009.
8. Karageorgiou, V., and Kaplan, D. Porosity of 3D biomaterial scaffolds and osteogenesis. Biomaterials **26,** 5474, 2005.
9. Levine, B. A new era in porous metals: applications in orthopaedics. Adv Eng Mater **10,** 788, 2008.
10. Singh, R., Lee, P.D., Lindley, T.C., Dashwood, R.J., Ferrie, E., and Imwinkelried, T. Characterization of the structure and permeability of titanium foams for spinal fusion devices. Acta Biomater **5,** 477, 2009.
11. Degasne, I., Basle, M.F., Demais, V., Hure, G., Lesourd, M., Grolleau, B., *et al.* Effects of roughness, fibronectin and vitronectin on attachment, spreading, and proliferation of human osteoblast-like cells (Saos-2) on titanium surfaces. Calcif Tissue Int **64,** 499, 1999.
12. Zanetti, A.S., McCandless, G.T., Chan, J.Y., Gimble, J.M., and Hayes, D.J. Characterization of novel akermanite:poly-ε-caprolactone scaffolds for human adipose-derived stem cells bone tissue engineering. J Tissue Eng Regen Med 2012. DOI: 10.1002/term.1646. [Epub ahead of print.]
13. Yeh, J.C., and Tucker, N. The use of tisseel in oculoplastics. Invest Ophthalmol Vis Sci **46,** 4252, 2005.
14. Topart, P., Vandenbroucke, F., and Lozac'h, P. Tisseel versus tack staples as mesh fixation in totally extraperitoneal laparoscopic repair of groin hernias. Surg Endosc **19,** 724, 2005.
15. Gertzman, A.A., and Sunwoo, M.H. Malleable paste for filling bone defects. Google Patents, 2000.
16. Otsu, N. A threshold selection method from gray-level histograms. Automatica **11,** 23, 1975.
17. Liu, Q., Cen, L., Yin, S., Chen, L., Liu, G., Chang, J., *et al.* A comparative study of proliferation and osteogenic differentiation of adipose-derived stem cells on akermanite and β-TCP ceramics. Biomaterials **29,** 4792, 2008.
18. Livak, K.J., and Schmittgen, T.D. Analysis of relative gene expression data using real-time quantitative PCR and the 2(-Delta Delta C(T)) method. Methods **25,** 402, 2001.
19. Aust, L., Devlin, B., Foster, S., Halvorsen, Y., Hicok, K., Du Laney, T., *et al.* Yield of human adipose-derived adult stem cells from liposuction aspirates. Cytotherapy **6,** 7, 2004.
20. Lopez, M.J., McIntosh, K.R., Spencer, N.D., Borneman, J.N., Horswell, R., Anderson, P., *et al.* Acceleration of spinal fusion using syngeneic and allogeneic adult adipose derived stem cells in a rat model. J Orthop Res **27,** 366, 2009.
21. Ho, S.T., and Hutmacher, D.W. A comparison of micro CT with other techniques used in the characterization of scaffolds. Biomaterials **27,** 1362, 2006.
22. Qureshi, A.T., Monroe, W.T., Dasa, V., Gimble, J.M., and Hayes, D.J. miR-148b–Nanoparticle conjugates for light mediated osteogenesis of human adipose stromal/stem cells. Biomaterials **34,** 7799, 2013.
23. Milat, F., and Ng, K.W. Is Wnt signalling the final common pathway leading to bone formation? Mol Cell Endocrinol **310,** 52, 2009.
24. Burge, R., Dawson-Hughes, B., Solomon, D.H., Wong, J.B., King, A., and Tosteson, A. Incidence and economic burden of osteoporosis-related fractures in the United States, 2005–2025. J Bone Miner Res **22,** 465, 2007.

25. Schulte, F.A., Ruffoni, D., Lambers, F.M., Christen, D., Webster, D.J., Kuhn, G., *et al.* Local mechanical stimuli regulate bone formation and resorption in mice at the tissue level. PLoS One **8,** e62172, 2013.
26. Gaalen, Sv., Kruyt, M., Meijer, G., Mistry, A., Mikos, A., Beucken, J.V.D., *et al.* Chapter 19: tissue engineering of bone. In: Clemens van, B., Peter, T., Anders, L., Jeffrey, H., David, F.W., Ranieri, C., *et al.*, eds. Tissue Engineering. Burlington: Academic Press, 2008, pp. 559–610.
27. Rydholm, A.E., Held, N.L., Benoit, D.S.W., Bowman, C.N., and Anseth, K.S. Modifying network chemistry in thiol-acrylate photopolymers through postpolymerization functionalization to control cell-material interactions. J Biomed Mater Res A **86A,** 23, 2008.
28. Rydholm, A.E., Reddy, S.K., Anseth, K.S., and Bowman, C.N. Controlling network structure in degradable thiol-acrylate biomaterials to tune mass loss behavior. Biomacromolecules **7,** 2827, 2006.
29. Bounds, C.O., Upadhyay, J., Totaro, N., Thakuri, S., Garber, L., Vincent, M., *et al.* Fabrication and characterization of stable hydrophilic microfluidic devices prepared via the *in situ* tertiary-amine catalyzed michael addition of multifunctional thiols to multifunctional acrylates. ACS Appl Mater Interfaces **5,** 1643, 2013.
30. Qureshi, A.T., Terrell, L., Monroe, W.T., Dasa, V., Janes, M.E., Gimble, J.M., *et al.* Antimicrobial biocompatible bioscaffolds for orthopaedic implants. J Tissue Eng Regen Med **8,** 386, 2014.
31. Barby, D., and Haq, Z. Low density porous cross-linked polymeric materials and their preparation and use as carriers for included liquids. Google Patents, 1985.
32. Lawrence, B.J., and Madihally, S.V. Cell colonization in degradable 3D porous matrices. Cell Adh Migr **2,** 9, 2008.
33. Di Maggio, N., Piccinini, E., Jaworski, M., Trumpp, A., Wendt, D.J., and Martin, I. Toward modeling the bone marrow niche using scaffold-based 3D culture systems. Biomaterials **32,** 321, 2011.
34. Scherberich, A., Galli, R., Jaquiery, C., Farhadi, J., and Martin, I. Three-dimensional perfusion culture of human adipose tissue-derived endothelial and osteoblastic progenitors generates osteogenic constructs with intrinsic vascularization capacity. Stem Cells **25,** 1823, 2007.
35. Papadimitropoulos, A., Scherberich, A., Guven, S., Theilgaard, N., Crooijmans, H.J., Santini, F., *et al.* A 3D *in vitro* bone organ model using human progenitor cells. Eur Cell Mater **21,** 445, 2011.
36. Mehrkens, A., Muller, A.M., Schafer, D., Jakob, M., Martin, I., and Scherberich, A. Towards an intraoperative engineering of osteogenic grafts from the stromal vascular fraction of human adipose tissue. Swiss Med Weekly **139,** 23S, 2009.
37. Bernhardt, A., Despang, F., Lode, A., Demmler, A., Hanke, T., and Gelinsky, M. Proliferation and osteogenic differentiation of human bone marrow stromal cells on alginate-gelatine-hydroxyapatite scaffolds with anisotropic pore structure. J Tissue Eng Regen Med **3,** 54, 2009.
38. He, J., Genetos, D.C., and Leach, J.K. Osteogenesis and trophic factor secretion are influenced by the composition of hydroxyapatite/poly(lactide-co-glycolide) composite scaffolds. Tissue Eng Part A **16,** 127, 2010.
39. Zhang, R., and Ma, P.X. Poly(alpha-hydroxyl acids)/hydroxyapatite porous composites for bone-tissue engineering. I. Preparation and morphology. J Biomed Mater Res **44,** 446, 1999.
40. Reynaud, E., Jouen, T., Gauthier, C., Vigier, G., and Varlet, J. Nanofillers in polymeric matrix: a study on silica reinforced PA6. Polymer **42,** 8759, 2001.
41. Ahn, S.H., Kim, S.H., and Lee, S.G. Surface-modified silica nanoparticle-reinforced poly (ethylene 2, 6-naphthalate). J Appl Polym Sci **94,** 812, 2004.

Address correspondence to:
Daniel. J. Hayes, PhD
Department of Biological Engineering
Louisiana State University Agricultural Center
149 E.B. Doran Building-Louisiana State University
Baton Rouge, LA 70803

E-mail: danielhayes@lsu.edu

Received: January 8, 2014
Accepted: August 15, 2014
Online Publication Date: September 18, 2014